Zinc blende-oxide phase transformation upon oxygen annealing of ZnSe shell in ZnO-ZnSe core-shell nanowires

S. Jabri, G. Amiri, S. Hassani, A. Lusson, V. Sallet, A. Meftah, P. Galtier, M. Oueslati

Zinc blende-oxide phase transformation upon oxygen annealing of ZnSe shell in ZnO-ZnSe core-shell nanowires

S. Jabri,[1,a)] G. Amiri,[2] S. Hassani,[2] A. Lusson,[2] V. Sallet,[2] A. Meftah,[1] P. Galtier,[2] and M. Oueslati[1]

[1]*Unité des nanomatériaux et photoniques, Faculté des Sciences de Tunis, Campus Universitaire Ferhat Hachad, El Manar, 2092 Tunis, Tunisie*

[2]*Groupe d'Etude de la Matière Condensée, CNRS-Université de Versailles St-Quentin-en-Yvelines, Université Paris-Saclay, 45 avenue des Etats Unis, 78035 Versailles Cedex, France*

(Received 24 December 2016; accepted 21 February 2017; published online 7 March 2017)

ZnO-ZnSe core-shell nanowires have been grown by metal organic chemical vapor deposition and subsequently annealed in an O_2 atmosphere. It has been found that the incorporation of oxygen into the ZnSe shell over the 470–580 °C temperature range results in a phase transformation from zinc Blende to orthorhombic and wurtzite. The X-ray diffraction pattern confirms that the heterostructures are composed of a wurtzite ZnO core and an oxide ZnSeO shell. The Raman spectroscopy study shows the appearance of additional peaks at 220 cm^{-1}, 278 cm^{-1}, 480 cm^{-1}, 550 cm^{-1}, and 568 cm^{-1}, which reveal a phase transformation associated with the incorporation of the oxygen into the shell after annealing at 470 °C. This work opens a way to study the structure stability of ZnO-ZnSe core-shell nanowire production and help to understand the mechanisms of the oxidation in ZnO-ZnSe core-shell nanowires. *Published by AIP Publishing.*
[http://dx.doi.org/10.1063/1.4977943]

In recent years, the core-shell structure nanowires (NWs) with type II band offsets have been a profitable scientific enterprise and have been considered to be the building blocks for the development of the next generation of solar energy conversion devices, due to their high efficiency in charge carrier transport and surface charge carrier transfer/separation.[1–6] Given that ZnO nanowires are one of the most important metal oxides, they are widely used as photo anode materials because they have a longer carrier lifetime and a higher electronic mobility. However, ZnO cannot absorb visible light and so only 3–5% of the solar spectrum reaching the earth can be used due to its wide band gap. Heterostructures are a promising means for improving the optical absorption capacity of ZnO. ZnSe is an ideal option for producing type-II ZnO heterostructures due to its relatively narrow band gap (2.7 eV).[5,7] The heteroepitaxial growth of the ZnSe shell has an inevitable problem associated. This problem stems from the difference in the thermal expansion coefficients and lattice constants of the ZB-ZnSe shell and the WZ-ZnO core.[8,9] The ZnSe shell grown on the ZnO nanowires using the metal organic chemical vapor deposition (MOCVD) growth technique induces a source of strain and structural defects that hamper the performance of the associated devices. Usually, the quality of these heterostructures on the ZnO-ZnSe interface is improved by increasing the degree of crystallinity and reducing the dislocation effects through annealing treatment. However, the thermal structure stability of the ZnSe shell has not been studied yet due to the novelty of this research field; furthermore, the heating up the heterostructures in such atmospheric gases may change their properties due to the oxygen reaction. The effect of oxygen could be the main cause for the unexpected discrepancies obtained in the structural and optical properties of the ZnSe shell. The occurrence of other nanostructures can be explained from a thermodynamic point of view.

In this work, the structural and optical properties of ZnSe-ZnO core-shell nanowire heterostructures grown by metal organic chemical vapor deposition (MOCVD) and subsequently annealed in an O_2 atmosphere are presented. An annealing study of the incorporation of oxygen into the ZnSe shell was carried out in order to investigate the influence of the O atoms on the phonon modes of the ZnSe zinc Blende.

The ZnO-ZnSe core-shell nanowires under investigation were grown by two steps, using metal organic chemical vapor deposition (MOCVD). The ZnO nanowire arrays were grown in a horizontal reactor of atmospheric pressure under N_2 carrier gas on a sapphire substrate at 900 °C. The nanowire array then served as a template for further ZnSe coating in a vertical reactor at 380 °C. Post-growth annealing was also achieved. The material was annealed in O_2 for 45 min from 470 to 600 °C.

The morphology of the core-shell nanowires was studied by scanning electron microscopy (SEM). The possible changes in core-shell nanowire structures during the post-annealing process were investigated by X-ray diffraction (XRD) using Cu Kα radiation ($\lambda = 0.154178$ nm) in the 2θ range of 25–40. The optical characteristics of the heterostructures were then analyzed by Raman spectroscopy at room temperature using an argon ion laser ($\lambda = 488$ nm). The excitation power laser was 2 mW on the surface of the sample. Additionally, a UV–visible spectrophotometer (Perkin

a)Author to whom correspondence should be addressed. Electronic mail: slaheddine.jabri@fst.rnu.tn. Tel.: (00216)55191507. Fax: (00216)71885073. Present address: Université de Tunis El Manar, Faculté des Sciences de Tunis, Département de Physique, Unité de nanomatériaux et photoniques, Tunis, Tunisia.

Elmer Lambda 950) was used to measure and compare the transmission spectra of both ZnO-ZnSe core-shell nanowires before and after annealing in an O_2 atmosphere.

Figure 1(a) presents a typical SEM image of a ZnO nanowire array grown on a sapphire substrate. The nanowires have smooth lateral surfaces. Their diameter is about 200–300 nm, while their length is several micrometers. Figure 1(b) shows that the ZnO nanowires are uniformly coated with a 100 nm ZnSe layer. Compared to the bare ZnO nanowire, a noticeable increase in the diameter and rough surface of ZnO-ZnSe nanowires was seen, which implies that ZnSe is deposited over the ZnO nanowires, making their diameter range from 400 to 500 nm.

Figure 2 shows the XRD pattern of the core and shelled ZnO nanowires as grown and annealed at 470 °C, 500 °C, 530 °C, 550 °C, 580 °C, and 600 °C. Fine XRD scans show a significant intensity decrease in the peak at $2\theta = 27.30°$ (111), indicating a decrease in the ZnSe amount deposited on the ZnO nanowires with the increase in the annealing temperature. Therefore, compared with the as-gown heterostructures, the shell annealed at 470 °C under O_2 has more additional crystallographic structures than zinc Blende, as evidenced by appearance of additional diffraction peaks. Two phases were then found to indicate the formation of $ZnSeO_3$ and ZnO during annealing. The additional peaks at $2\theta = 32.34°$ (210) and 33.04° (121) correspond to the $ZnSeO_3$ phase.[10] Furthermore, a peak of ZnO at 31.8° (10–10) was observed in the curve (470 °C), which means that ZnO and $ZnSeO_3$ could be thermodynamically formed in the ZnSe shell. This is in accordance with Gunchenko *et al.*[11] who reported that the oxidation of ZnSe follows this mechanism:

$$2\,\mathrm{ZnSe} + \mathrm{O2} \rightarrow 2\,\mathrm{ZnO} + 2\,\mathrm{Se}\uparrow$$
$$2\,\mathrm{ZnSe} + 3\,\mathrm{O_2} \rightarrow 2\,\mathit{ZnSe}\mathrm{O_3}.$$

At annealing temperatures of more than 580 °C, no oxide phases were detected. Only the strong hexagonal ZnO (0002) diffraction peak was observed in the XRD patterns; its intensity is greater than that of the as-grown sample because both the ZnSe and ZnOSe shells are removed at a temperature of more than 580 °C. Thus, the ZnO-ZnSe core-shell heterostructures are transformed into ZnO-ZnOSe and then into just ZnO as a result of an annealing effect.

In order to obtain detailed information about the phase structure of the as-synthesized ZnO-ZnSe heterostructures, Raman scattering measurements were used to obtain additional data about defect evolution during the annealing process as shown below. The Wurtzite-type ZnO belongs to the C_{6v}^4 space group. The zone-center optical phonons can be classified according to the following irreducible representations: $\Gamma_{opt} = A_1 + E_1 + 2E_2 + 2B_1$. Regarding the optical modes, the B_1 modes are silent modes, and the A_1 and E_1 are polar modes and are split into transverse optical (TO) and longitudinal optical (LO) phonons. A nonpolar phonon mode with E_2 symmetry has two frequencies E_2 (High) and E_2 (Low) and is associated with oxygen and Zinc atom sublattices, respectively. Among the optical modes, A_1, E_1, and E_2 are Raman active.[12] The crystal structure of ZnSe is a zinc Blende (T_d). The zone-center optical phonons can be classified according to the following irreducible representations: $\Gamma_{opt} = A_1 + E_1$. This structure involves two Raman active phonon modes in which the LO and TO symmetries are Raman active.[13]

Figure 3(a) shows Raman spectra prior to and after the annealing of the ZnO-ZnSe core-shell nanowires. In the as-grown ZnO-ZnSe core-shell, TO (205 cm^{-1}) and LO (250 cm^{-1}) peaks of the ZnSe shell are observed in the curve of the as-grown sample. These phonon modes, which are allowed and observed in the backscattering, that arises from the (111) orientation, have shown that the ZnSe shell has a zinc-Blende structure along the [111] direction. The high volume ratio of ZnO-ZnSe ($\frac{V_{shell\,ZnSe}}{V_{core\,ZnO}}$) makes the ZnO core modes unobservable in the Raman spectra. At annealing temperatures of less than 470 °C, no oxide phases have been detected. After annealing at a temperature, T, of more than 580 °C, the peaks at 330 cm^{-1} and 438 cm^{-1}, which correspond to ($E_2^{high} - E_2^{low}$) and E_2^{high} of the ZnO core,

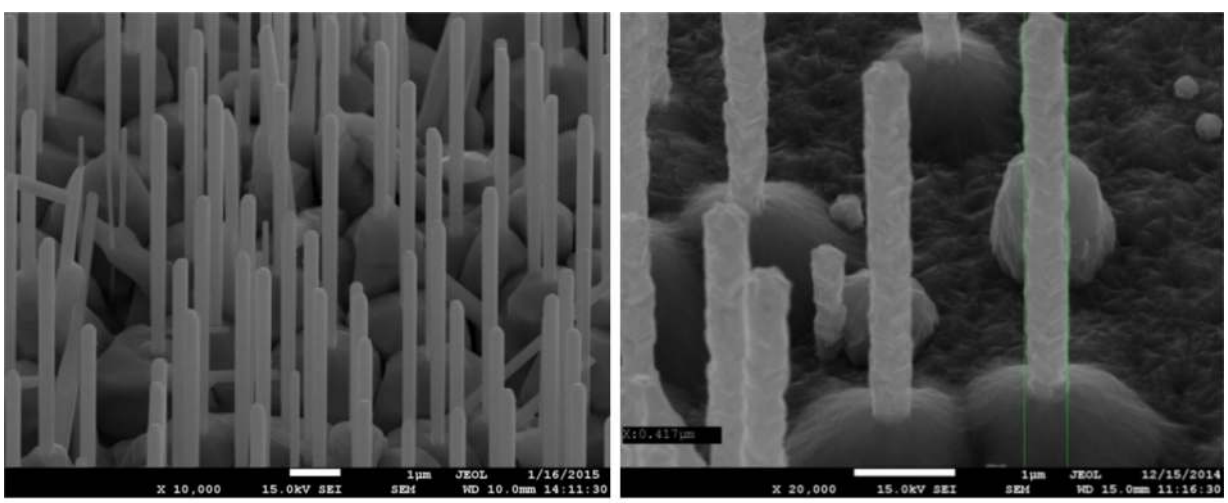

(a) (b)

FIG. 1. (a) SEM image of a well-aligned ZnO nanowire array grown on sapphire. The average length of the nanowires is about 3 μm and the diameters are about 200–300 nm. (b) SEM image of the well-aligned ZnO-ZnSe core-shell nanowire array grown by MOCVD.

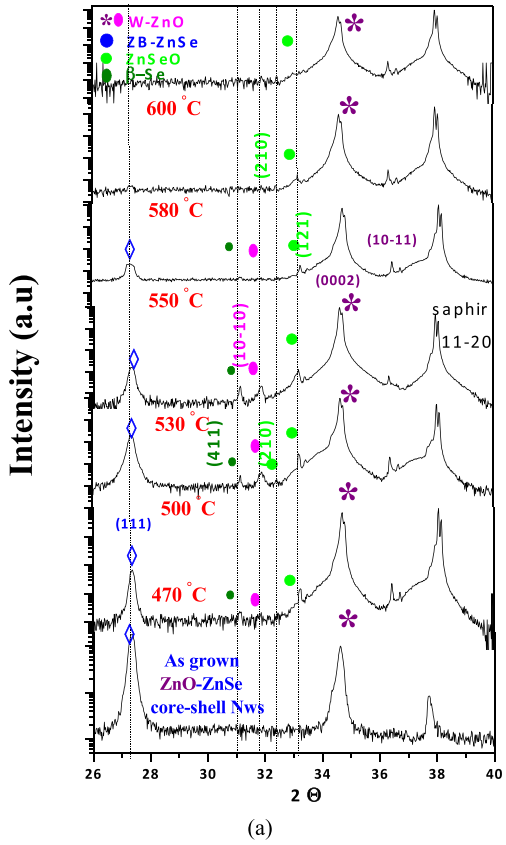

(a)

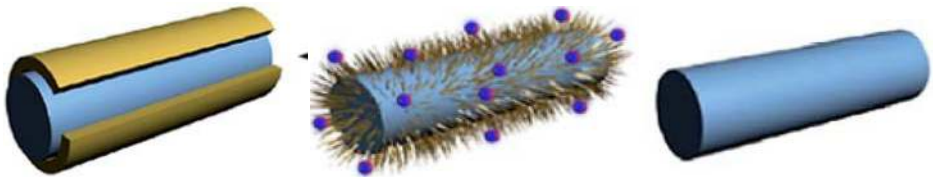

(b)

FIG. 2. (a) XRD patterns of ZnO–ZnSe before and after annealing at 470 °C, 500 °C, 530 °C, 550 °C, 580 °C, and 600 °C. (b) Schematic illustration of the transformation of the ZnO-ZnSe core shell nanowires (before annealing) into a ZnO-ZnSeO oxide (at temperature range 470–580 °C) and then only ZnO nanowires (temperature higher than 580 °C).

respectively, are clearly observed and all the ZnSe Raman peaks have disappeared. However, three peaks appear at 278 cm^{-1}, 480 cm^{-1}, and 568 cm^{-1} in the annealing temperature range [470–580 °C]. The appearance of these bands could be thusly explained:

On the one hand, it is believed that the location of the peak at 550 cm^{-1} is due to the substitution of O onto the Se atom sites in the ZnSe shell to form new ZnSeO oxide phases. Given that the oxygen atom is much lighter than the selenium atom it replaces, its LO phonon frequency of vibration increases by a factor of a square root of $\omega_{Zn-O} = \omega_{LO}\sqrt{\frac{mSe}{mO}}$.[14] (Assuming that the Zn-O spring constant remains similar to that of the Zn-Se) compared to ZnSe. With the Zn-Se LO frequency equal to 250 cm^{-1}, the Zn−O LO frequency is estimated to be 555 cm^{-1}, close to the 550 cm^{-1} observed in the Raman spectra mentioned above. Due to the foreign O-atom, three additional phonon modes at 220 cm^{-1}, 480 cm^{-1}, and 550 cm^{-1} emerge from the cubic structure because the oxidation has turned the ZnSe shell from the cubic phase to the orthorhombic phase according to the XRD results.

The exact peak positions are shown in Fig. 3(b) by fitting the data with a Lorentzian curve. In the annealed samples, the TO of the ZnSe vibrational mode shifted to higher wavenumbers and occurred at 220 cm^{-1}. This amounts to a host impurity shift of 15 cm^{-1} for the vibrational mode at 205 cm^{-1}. In fact, the deformation potential interaction is proportional to the deformation constant, which depends on the difference between the impurity and the host atom radii δR.[15] Given that the Se anions are smaller than the O anions, the substitution of Se for O increases the atomic size difference $|r_{Se\ r_O}|$ and results in tensile strain in the sublattice along the [111] direction. Concerning the appearance of the band at 480 cm^{-1}, it is caused by the high density of the defects introduced by annealing, which cut the long range lattice ordering. The Raman selection rules are therefore relaxed and many other phonon modes, which are forbidden in the perfect lattice, participate in the Raman spectrum, thus contributing to the broad peak at 480 cm^{-1}.

When increasing the annealing temperature, the selenium atom moves to form a vacancy site and is then ejected from the growth shell. The oxygen atom is expected to have

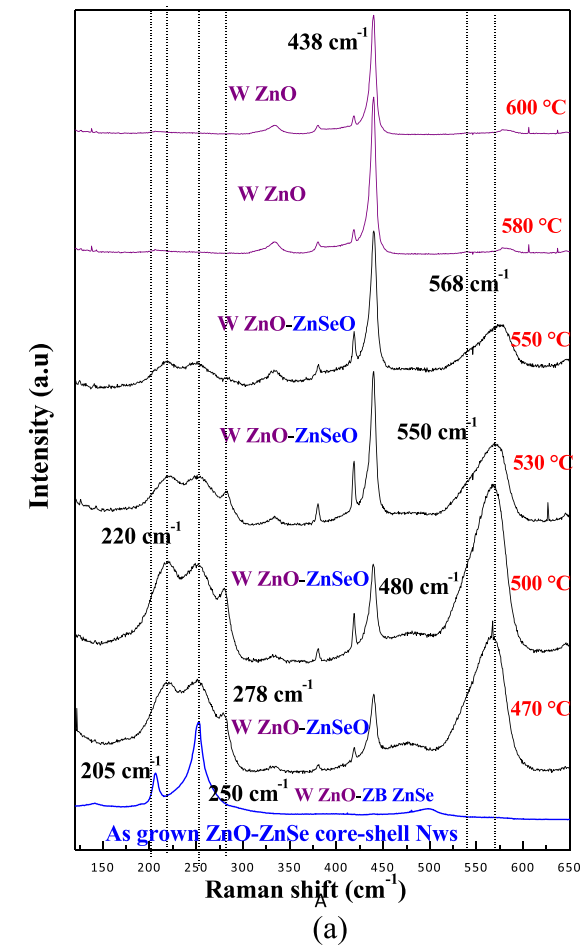

FIG. 3. (a) Raman spectra of ZnO-ZnSe nanowires on a sapphire substrate, as a function of annealing temperature under O_2. (b) The optical phonon frequencies of ZnO-ZnSe nanowires at temperature 500 °C.

a higher surface mobility and will then be more efficiently incorporated into the zinc-blende shell structure to replace the selenium and link with the zinc. Therefore, by increasing the annealing temperature to 580 °C, the overall proportion of the ZnSeO phase is effectively being raised while reducing the ZnSe phase correlated with the decrease in the Raman intensity of the LO mode at 250 cm^{-1} corresponding to ZnSe zinc Blende phase.

On the other hand, *Gunchenko* et al.[11] reported that the oxidation of ZnSe is accompanied by a decrease in the weight of the sample. This decrease in weight can be attributed to the formation of ZnO that is conjoined with a sublimation of Se, which is highly volatile. The phase abundance of ZnO is greater than that of $ZnSeO_3$, which means that the formation of ZnO is more thermodynamically favorable than the $ZnSeO_3$ formation at 470 °C. It is clear that the rate of oxidation increases as the temperature gets higher and the rate of formation of ZnO is much higher than that of ZnSeO3. This is in agreement with the thermodynamic calculations which found that the free energy ($-\Delta G$) of the ZnO formation is 242.6 kJ/mole, while that of $ZnSeO_3$ formation is 393 kJ/ mole.[16,17] The reflection peak observed at (10–10) confirms the existence of the ZnO phase. The additional peaks at 278 cm^{-1} and 568 cm^{-1} remind us of the history of local vibration modes (LVMs) in doped ZnO. Indeed, these bands could be attributed to LVMs of selenium impurities that existed in a formed ZnO phase. Many reports have evidenced some intrinsic defects to be associated with the presence of the Raman mode at around 278 and 580 cm^{-1} in the ZnO structure. These modes have been observed at different wavenumbers from 273 to 280 cm^{-1} and 570 to 582 cm^{-1} in ZnO after doping with different elements. In fact, these values were observed in the spectra of Fe, Sb, Ga Al, and N-doped ZnO thin films.[18–20] The authors attributed the common anomalous bands to intrinsic host-lattice defects related to doping. At a temperature of 580 °C, all selenium impurities are sublimated, and the shell is totally removed from the ZnO core to leave only an undoped ZnO phase.

To further demonstrate the phase transformation of the ZnSe shell observed in the ZnO-ZnSe heterostructure samples, UV-vis absorption has also been used to measure the absorption regions in the ZnSeO sample as a function of annealing temperature. The transmission spectra of the ZnO-ZnSe core-shell NWs and their derivative curves are, respectively, shown in Fig. 4(a). The transmission spectra reveal significant differences in the optical absorption properties of the ZnO-ZnSe heterostructures before and after annealing. However, the transmission gradually extends from the visible region to the ultraviolet region and increases in intensity with the increasing temperature. Derivative-curves of the transmission spectrum for the core-shell nanowires are shown in Fig. 4(b) in order to clearly observe the absorption peak. Before annealing, only a strong absorption is seen in the visible region at 2.7 eV, which is a characteristic of the band-gap of ZB-ZnSe semiconductor materials. After annealing at 500 °C, only a peak is observed at 3.33 eV, emanating from the W-ZnO near-band edge (NBE).[21,22] The band gap energy of the ZnSe shell remains constant with the addition of an amount of oxygen to the ZnSe shell. This is evidenced by a direct comparison between the as-grown and the annealed samples at 500 °C.

Although the results above indicate that the phase of the ZnSe shell changed upon annealing of the ZnO-ZnSe core-shell in O_2, the occurrence of oxide phases after oxygen substitution in the lattice sites, as well as the oxygen-incorporation into the ZnSe shell during the annealing

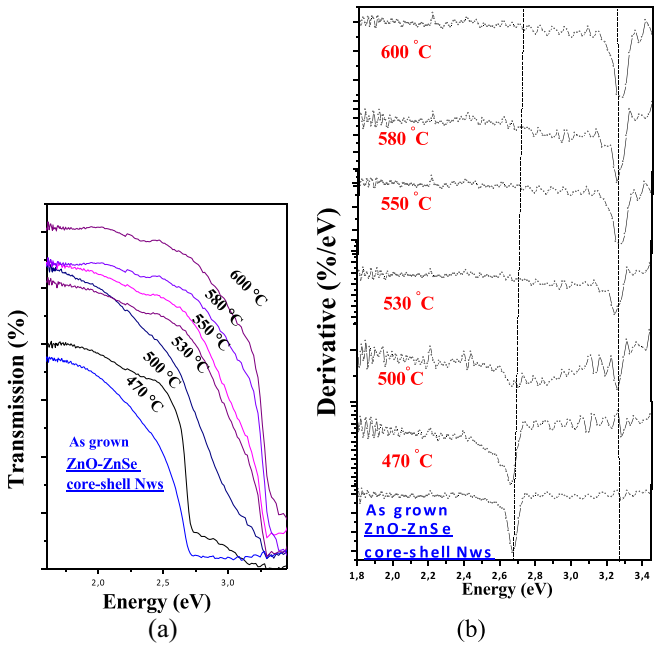

FIG. 4. (a) Transmission spectra of ZnO-ZnSe core-shell nanowires before and after annealing. (b) The derivative curves show two vertical lines that indicate the near band edge (NBE) absorption peaks from ZnO and ZnSe on annealing.

operation, does not modify the local electronic structure as evidenced by *Broesler et al.*[23]

The ZnO-ZnSe core-shell nanowires have been grown by MOCVD. The evolution of their structural and optical properties with respect to annealing temperatures has been studied. The incorporation of oxygen has resulted in a phase transformation from zinc Blende ZnSe to zinc Selenite ZnSeO and ZnO shell. XRD results have shown new peaks at 33.04° and 32.34° that indicate a ZnSeO phase after oxidation at a temperature higher than 470 °C. Four observed Raman peaks at 278 cm^{-1}, 480 cm^{-1}, 550 cm^{-1}, and 568 cm^{-1} have been attributed to the vibration modes of the substituted oxygen atom in the zinc blend phase and the oxide phase. These experimental results confirm the replacement of Se anions in ZnSe for oxygen in the lattice site and further confirm that isoelectronic oxygen does not form a mismatched alloy system in the ZnSeO shell.

[1]Y. Cao, Z. Wu, J. Ni, W. A. Bhutto, J. Li, S. Li, and J. Kang, Nano-Micro Lett. **4**(3), 135–141 (2012).
[2]X. Zhang, M. Chen, J. Wen, L. Wu, H. Gao, and D. Zhang, CrystEngComm **15**(10), 1908–1913 (2013).
[3]Z. Wu, Y. Zhang, J. Zheng, X. Lin, X. Chen, B. Huang, and J. Kang, J. Mater. Chem. **21**(16), 6020–6026 (2011).
[4]N. Liang, M. Wang, L. Jin, S. Huang, W. Chen, M. Xu, Q. He, J. Zai, N. Fang, and X. Qian, ACS Appl. Mater. Interfaces **6**, 11698–11705 (2014).
[5]K. Wang, J. Chen, W. Zhou, Y. Zhang, Y. Yan, J. Pern, and A. Mascarenhas, Adv. Mater. **20**(17), 3248–3253 (2008).
[6]Y. Zhang, L. W. Wang, and A. Mascarenhas, Nano Lett. **7**(5), 1264–1269 (2007).
[7]Y. Myung, J. H. Kang, J. W. Choi, D. M. Jang, and J. Park, J. Mater. Chem. **22**(5), 2157–2165 (2012).
[8]S. Gul, J. K. Cooper, P. A. Glans, J. Guo, V. K. Yachandra, J. Yano, and J. Z. Zhang, ACS Nano. **7**(10), 8680–8692 (2013).
[9]C. W. Na, S. Y. Park, J. H. Chung, and J. H. Lee, ACS Appl. Mater. Interfaces **4**(12), 6565–6572 (2012).
[10]K. Kohn, K. Inoue, O. Horie, and S. I. Akimoto, J. Solid State Chem. **18**(1), 27–37 (1976).
[11]N. N. Gunchenko, G. N. Dronova, I. A. Maksimova, I. A. Mironova, V. N. Pavlova, and N. I. Pevtsova, Inorg. Mater. **24**(1) (1988).
[12]S. Jabri, H. Souissi, A. Souissi, A. Meftah, V. Sallet, A. Lusson, and M. Oueslati, J. Raman Spectrosc. **46**(2), 251–255 (2015).
[13]S. Jabri, G. Amiri, V. Sallet, A. Souissi, A. Meftah, P. Galtier, and M. Oueslati, Physica B **489**, 93–98 (2016).
[14]X. Zhang, D. Wang, M. Beres, L. Liu, Z. Ma, Y. Y. Peter, and S. S. Mao, Appl. Phys. Lett. **103**(8), 082111 (2013).
[15]J. W. Allen, Journal of Physics C: Solid State Physics **1**(4), 1136 (1968).
[16]W. M. Jim and E. J. Stofko, J. Electrochem. Soc. **119**, 381 (1972).
[17]Z. K. Heiba, Powder Diffraction **17**(3), 191–195 (2002).
[18]J. Duan, H. Wang, H. Wang, J. Zhang, S. Wu, and Y. Wang, CrystEngComm. **14**(4), 1330–1336 (2012).
[19]A. Kaschner, U. Haboeck, M. Strassburg, M. Strassburg, G. Kaczmarczyk, A. Hoffmann, C. Thomsen, A. Zeuner, H. R. Alves, D. M. Hofmann, and B. K. Meyer, Appl. Phys. Lett. **80**(11), 1909–1911 (2002).
[20]M. A. Gluba, N. H. Nickel, and N. Karpensky, Phys. Rev. B **88**(24), 245201 (2013).
[21]L. Sun, Z. Ye, and H. He, Nanoscale **7**(16), 7299–7306 (2015).
[22]W. Chen, N. Zhang, M. Y. Zhang, X. T. Zhang, H. Gao, and J. Wen, CrystEngComm **16**(6), 1201–1206 (2014).
[23]R. Broesler, E. E. Haller, W. Walukiewicz, T. Muranaka, T. Matsumoto, and Y. Nabetani, Appl. Phys. Lett. **95**(15), 151907 (2009).